Draft version February 5, 2008
Preprint typeset using LaTeX style emulateapj v. 6/22/04

THE NON-GAUSSIAN COLD SPOT IN THE 3-YEAR WMAP DATA

M. Cruz[1]
IFCA, CSIC-Univ. de Cantabria, Avda. los Castros, s/n,
E-39005-Santander,
Spain

L. Cayón
Department of Physics, Purdue University, 525 Northwestern Avenue, West Lafayette,
IN 47907-2036, USA

E. Martínez-González
IFCA, CSIC-Univ. de Cantabria, Avda. los Castros s/n,
39005-Santander,Spain

P. Vielva[2]
IFCA, CSIC-Univ. de Cantabria, Avda. los Castros, s/n,
39005-Santander,Spain

and

J. Jin
Department of Statistics. Purdue University. 150 N. University Street, West Lafayette,
IN 47907-2067

Draft version February 5, 2008

ABSTRACT

The non-Gaussian cold spot detected in wavelet space in the WMAP 1–year data, is detected again in the coadded WMAP 3–year data at the same position ($b = -57°, l = 209°$) and size in the sky ($\approx 10°$). The present analysis is based on several statistical methods: kurtosis, maximum absolute temperature, number of pixels below a given threshold, volume and Higher Criticism. All these methods detect deviations from Gaussianity in the 3–year data set at a slightly higher confidence level than in the WMAP 1–year data. These small differences are mainly due to the new foreground reduction technique and not to the reduction of the noise level, which is negligible at the scale of the spot. In order to avoid *a posteriori* analyses, we recalculate for the WMAP 3–year data the significance of the deviation in the kurtosis. The skewness and kurtosis tests were the first tests performed with wavelets for the WMAP data. We obtain that the probability of finding an at least as high deviation in Gaussian simulations is 1.85%. The frequency dependence of the spot is shown to be extremely flat. Galactic foreground emissions are not likely to be responsible for the detected deviation from Gaussianity.

Subject headings: methods: data analysis – cosmic microwave background

1. INTRODUCTION

The Cosmic Microwave Background (CMB) is at the moment the most useful tool in the study of the origin of the universe. A precise knowledge of its power spectrum constrains significantly the values of the cosmological parameters which determine the cosmological model. The 1–year Wilkinson Microwave Anisotropy Probe data (WMAP, Bennett et al. 2003a), measured the anisotropies of the CMB with unprecedented accuracy, finding that the standard model fits these data. A flat Λ–dominated Cold Dark Matter (ΛCDM) universe with standard inflation explains most of the observations confirming the widely accepted concordance model. According to standard inflation, the temperature anisotropies of the CMB are predicted to represent a homogeneous and isotropic Gaussian random field on the sky. A first Gaussianity analysis found the data to be compatible with Gaussianity (Komatsu et al. 2003).

Several non–Gaussian signatures or asymmetries were detected in the 1–year WMAP data in subsequent works. A variety of methods were used and applied in real, harmonic and wavelet space: low multipole alignment statistics (de Oliveira–Costa et al. 2004, Copi et al. 2004, 2005, Schwarz et al. 2004, Land & Magueijo 2005a,b,c, Bielewicz et al. 2005, Slosar & Seljak 2004); phase correlations (Chiang et al. 2003, Coles et al. 2004); hot and cold spot analysis (Larson & Wandelt 2004, 2005); local curvature methods (Hansen et al. 2004, Cabella et al. 2005); correlation functions (Eriksen et al. 2004a, 2005, Tojeiro et al. 2005); structure alignment statistics

[1] Also at Dpto. de Física Moderna, Univ. de Cantabria, Avda. los Castros, s/n, 39005-Santander, Spain
Electronic address: cruz@ifca.unican.es
Electronic address: cayon@physics.purdue.edu
Electronic address: martinez@ifca.unican.es
[2] Also at Astrophysics Group, Cavendish Laboratory, Madingley Road, Cambridge CB3 0HE, UK
Electronic address: vielva@ifca.unican.es
Electronic address: jinj@stat.purdue.edu

(Wiaux et al. 2006); multivariate analysis (Dineen & Coles 2005); Minkowski functionals (Park 2004, Eriksen et al. 2004b); gradient and dispersion analyses (Chyzy et al. 2005); and several statistics applied in wavelet space (Vielva et al. 2004, Mukherjee & Wang 2004, Cruz et al. 2005, 2006, McEwen et al. 2005a and Cayón, Jin & Treaster 2005).

The recently released 3–year WMAP data with higher signal to noise ratio is key to confirm or disprove all these results.

In the 3–year papers, the WMAP team (Hinshaw et al. 2006) re-evaluates potential sources of systematic errors and concludes that the 3–year maps are consistent with the 1–year maps. The exhaustive polarization analysis enhances the confidence on the accuracy of the temperature maps. The ΛCDM model continues to provide the best fit to the data.

Spergel et al. (2006) perform a Gaussianity analysis of the 3–year data. No departure from Gaussianity is detected based on the one point distribution function, Minkowski functionals, the bispectrum and the trispectrum of the maps. The authors do not re-evaluate the other statistics showing asymmetries or non–Gaussian signatures in the 1–year data.

The aim of this paper is to check the results of Vielva et al. (2004), Cruz et al. (2005), Cayón, Jin & Treaster (2005) and Cruz et al. (2006), (hereafter V04, C05, CJT and C06 respectively) with the recently released WMAP data. All these analyses were based on wavelet space. In particular the data were convolved with the Spherical Mexican Hat Wavelet (SMHW). Convolution of a CMB map with the SMHW at a particular wavelet scale increases the signal to noise ratio at that scale. Moreover, the spatial location of the different features of a map is preserved.

V04 detected an excess of kurtosis in the 1–year WMAP data compared to 10000 Gaussian simulations. This excess occurred at wavelet scales around 5° (angular size in the sky of $\approx 10°$). The excess was found to be localized in the southern Galactic hemisphere. A very cold spot, called *the Spot*, at galactic coordinates ($b = -57°, l = 209°$), was pointed out as the possible source of this deviation.

C05 showed that indeed *the Spot* was responsible for the detection. The number of cold pixels below several thresholds (cold Area) of *the Spot* was unusually high compared to the spots appearing in the simulations. Compatibility with Gaussianity was found when masking this spot in the data. The minimum temperature of *the Spot* was as well highly significant.

C06 confirmed the robustness of the detection and analysed the morphology and the foreground contribution to *the Spot*. *The Spot* appeared statistically robust in all the performed tests, being the probability of finding a similar or bigger spot in the Gaussian simulations less than 1%. The shape of *the Spot* was shown to be roughly circular, using Elliptical Mexican Hat Wavelets on the sphere. Moreover the foreground contribution in the region of *the Spot* was found to be very low. *The Spot* remained highly significant independently of the used foreground reduction technique. In addition the frequency dependence of *the Spot* was shown to be extremely flat. Even considering large errors in the foreground estimation it was not possible to explain the non-Gaussian properties of *the Spot*.

CJT applied Higher Criticism statistics (hereafter HC) to the 1–year maps after convolving them with the SMHW. This method provided a direct detection of *the Spot*. The HC values appeared to be higher than 99% of the Gaussian simulations.

Note that although *the Spot* has not been detected in real space, this structure exists but is hidden by structures at different scales. The convolution with the SMHW at the appropriate scale, amplifies *the Spot*, making it more prominent.

Several attempts have been made in order to explain the non-Gaussian nature of this cold spot. Tomita (2005) suggested that local second–order gravitational effects could produce *the Spot*. Inoue & Silk (2006) considered the possibility of explaining *the Spot* and other large scale anomalies by local compensated voids. Jaffe et al. (2005a) and Cayón et al. (2006) assumed an anisotropic Bianchi VII_h model showing that it could explain the excess of kurtosis and the HC detection as well as several large scale anomalies. On the other hand, McEwen et al. (2005b) still detect non-Gaussianity in the Bianchi corrected maps. Jaffe et al. (2005b) proved the incompatibility of the extended Bianchi models including the dark energy term with the 1–year data. Adler et al. (2006), developed a finite cosmology model which would explain *the Spot* and the low multipoles in the angular power spectrum. Up to date there are no further evidences of the validity of any of the above suggested explanations.

Our paper is organized as follows. We discuss the changes in the new WMAP data release and the simulations in section §2. The analysis using all the mentioned estimators is described in section §3. In section §4, the significance of our findings is discussed. We analyse the frequency dependence of *the Spot* in section §5, and our discussion and conclusions are presented in sections §6 and §7.

2. WMAP 3–YEAR DATA AND SIMULATIONS

The WMAP data are provided at five frequency-bands, namely K–band (22.8 GHz, one receiver), Ka–band (33.0 GHz, one receiver), Q–band (40.7 GHz, two receivers), V–band (60.8 GHz, two receivers) and W–band (93.5 GHz, four receivers). Foreground cleaned maps for the Q, V, and W channels are also available at the Legacy Archive for Microwave BAckground Data Analysis (LAMBDA) web site [3].

Most of the 1–year Gaussianity analyses were performed using the WMAP combined, foreground cleaned Q–V–W map (hereafter WCM; see Bennett et al. 2003a). CMB is the dominant signal at these bands and noise properties are well defined for this map. The de-biased Internal Linear Combination map, (DILC) proposed by the WMAP team, estimates the CMB on the whole sky. However its noise properties are complicated and regions close to the Galactic plane will be highly contaminated by foregrounds. Chiang, Naselsky & Coles (2006) find evidences for the foreground contamination of the DILC. Therefore we will still use the more reliable WCM in the 3–year data analysis.

Hinshaw et al. (2006) describe some changes in the 3–year temperature analysis with respect to the 1–year

[3] http://lambda.gsfc.nasa.gov

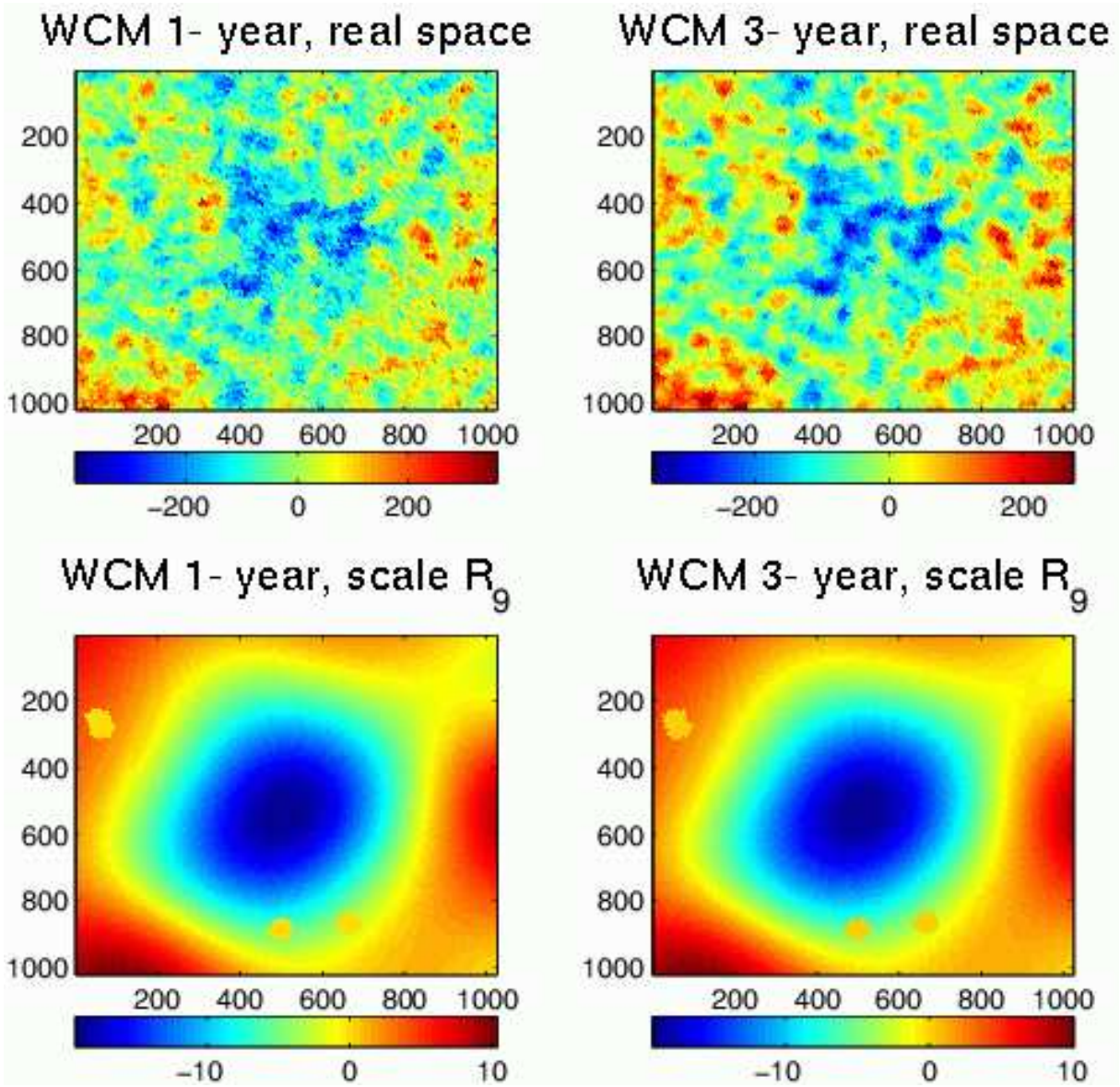

FIG. 1.— Image showing an azimuthal projection of a $22° \times 22°$ patch from the WCM HEALPix map with resolution nside = 256, centered on *the Spot* and in μK. In the first row we have the 1–year and 3–year images of *the Spot* in real space, whereas in the second row *the Spot* is shown at wavelet scale R_9. The image is divided in 1024×1024 pixels and the y-axis is oriented in the Galactic north-south direction.

one. Coadding the three years of observations reduces the instrumental noise. The 3–year maps have ≈ 3 times lower variance. Refinements in gain calibration and beam response models have been implemented and a new foreground reduction technique has been used. The latter seems to provide a better correction than the one applied to the first year data. As discussed in C06 the Galactic foreground estimation is a very important issue in Gaussianity analyses. The exclusion masks defined by Bennett et al. (2003b) have not been modified, except for the inclusion of 81 new point sources in the kp0 mask. This mask excludes the highly contaminated pixels close to the Galactic plane.

Despite these changes the 3–year maps have been found to be consistent with the 1–year maps by the WMAP team.

V04 and C05 performed a very careful analysis in order to study the power spectrum and noise dependence of the kurtosis and cold Area estimators. Considering different power spectra within the 1σ error band of the 1–year data, the differences in the significance of the kurtosis were found to be negligible (see Figure 11 in V04). The Area of a particular spot was neither affected by the power spectrum (see section 5.3 in C05). The results were almost noise independent. The convolution with the SMHW reduces considerably the noise contribution. Even if similar results are expected, we perform 10000 Gaussian simulations of the 3–year coadded data following the same steps as for the 1–year simulations. The only differences between the 3–year and the 1–year simulations are a lower noise contribution and a very slight variation in the power spectrum used to generate the

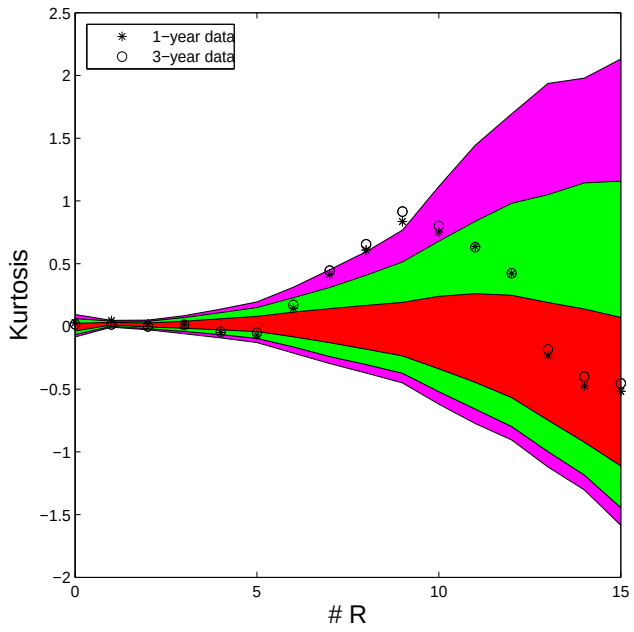

FIG. 2.— WCM kurtosis values for the 1–year (asterisks) and the 3–year data (circles). The acceptance intervals for the 32% (inner), 5% (middle) and 1% (outer) significance levels, given by the 10000 simulations are also plotted.

simulations. For a detailed description of the simulation pipeline, see section 2 of V04.

We will use all these maps in the HEALPix pixelisation scheme (Górski et al. 2005) [4] with resolution parameter Nside = 256.

3. ANALYSIS

Our aim in this section is to repeat the same tests performed in V04, C05, CJT and C06 but with the 3–year data. Then we will compare the new results to the old ones. One can see the region of *the Spot* in real and wavelet space at scale 5° for both releases of the WMAP data in Figure 1. In real space the 3–year data image appears clearly less noisy, whereas the wavelet space images present only very small differences.

In V04, data and simulations were convolved with the SMHW at 15 scales, namely ($R_1 = 13.7$, $R_2 = 25$, $R_3 = 50$, $R_4 = 75$, $R_5 = 100$, $R_6 = 150$, $R_7 = 200$, $R_8 = 250$, $R_9 = 300$, $R_{10} = 400$, $R_{11} = 500$, $R_{12} = 600$, $R_{13} = 750$, $R_{14} = 900$ and $R_{15} = 1050$ arcmin). The SMHW optimally enhances some non-Gaussian signatures on the sphere (Martínez–González et al. 2002) and has the following expression:

$$\Psi_S(y,R) = \frac{1}{\sqrt{2\pi}N(R)}\left[1+\left(\frac{y}{2}\right)^2\right]^2\left[2-\left(\frac{y}{R}\right)^2\right]e^{-y^2/2R^2},$$

where $N(R)$ is a normalisation constant: $N(R) \equiv R\sqrt{1+R^2/2+R^4/4}$. The distance y on the tangent plane is related to the polar angle (θ) as: $y \equiv 2\tan\theta/2$.

We will use the same 15 scales in our present analysis, considering those estimators where non-Gaussianity was found in the 1–year data, namely kurtosis, Area, *Max*, HC and a new one, the volume. The definitions of each estimator will be given in the following subsections. Analyses were also performed in real space, which will be referred as wavelet scale zero. In real space, the data are found to be compatible with Gaussian predictions

In the following subsections we will give the upper tail probabilities of the data at one particular scale. The upper tail probability is the probability that the relevant statistic takes a value at least as large as the one observed, when the null hypothesis is true.

In section §4 we will give a more rigorous measure of the significance, considering the total number of performed tests to calculate the p-value of *the Spot*. The p-value is the probability that the relevant statistic takes a value at least as extreme as the one observed, when the null hypothesis is true. In our case, the null hypothesis is the Gaussianity of the temperature fluctuations.

3.1. *Kurtosis*

Given a random variable X, the kurtosis κ is defined as $\kappa(X) = \frac{E[X^4]}{(E[X^2])^2} - 3$. In V04 the kurtosis of the wavelet coefficients was compared to the acceptance intervals given by the simulations. In Figure 2 the kurtosis of the 1–year data are represented by asterisks and the 3–year data by circles. Hereafter we will use these symbols to represent 1–year and 3–year data. Both are plotted versus the 15 wavelet scales. Scale 0 corresponds to real space. The acceptance intervals given by the simulations will be plotted in the same way in all figures: the 32% interval corresponds to the inner band, the 5% interval to the middle band and the 1% acceptance interval, to the outer one. As expected, the acceptance intervals remain almost unchanged with respect to those obtained from 1–year simulations. This will happen as well for all the other estimators. The 3–year kurtosis values follow the same pattern as the 1–year ones, confirming the initial results. However there are slight differences at the scales where the deviation is detected, being the kurtosis even higher in the 3–year data. The most significant deviation from the Gaussian values, occurs at scale $R_9 = 5°$. In Table 1 we list the kurtosis values at scale R_9, considering the 1–year data as published in 2003, the 1–year data release applying the changes in the data analysis described in Hinshaw et al.(2006), and the coadded 3–year data. The biggest difference is found between both releases of the 1–year data. The kurtosis value of the 1–year data increases $\approx 7\%$. This may be due to the new foreground reduction technique. As expected the noise reduction due to coadding the three years of observations, implies a much lower increase in the kurtosis, since the noise contribution in wavelet space is very small. The upper tail probabilities (i.e. the probabilities of obtaining higher or equal values assuming the Gaussian hypothesis) are given in the right column of Table 1. Hereafter we will compare the first release of the 1–year data with the 3–year data.

Analysing both Galactic hemispheres separately, we obtain the results presented in Figure 3. Again the kurtosis follows the same pattern as in the 1–year results. As expected, the deviation appears only in the southern hemisphere and it is slightly higher in the 3–year data. The upper tail probability obtained in V04 was 0.11% at scale R_7 in the southern hemisphere, whereas now we

[4] http://www.eso.org/science/healpix/

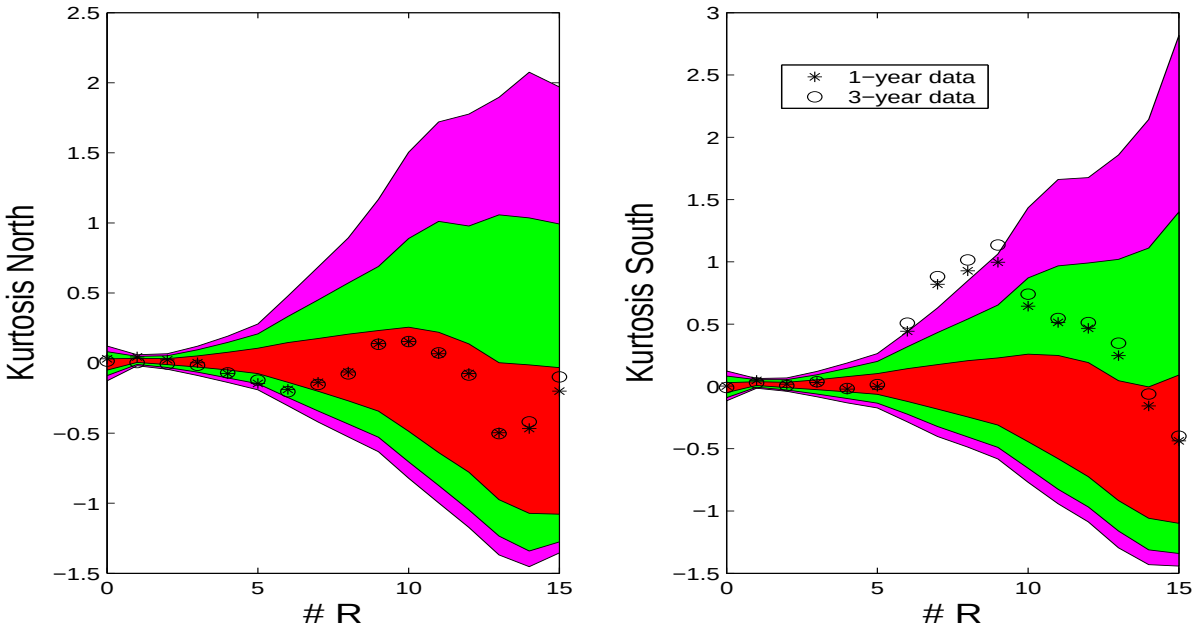

FIG. 3.— As in Figure 2 but for the northern (left plot) and southern (right plot) Galactic hemispheres.

TABLE 1
KURTOSIS VALUES AT SCALE R_9

Data	kurtosis	probability[a]
1–year data (2003)	0.836	0.38%
1–year data (2006)	0.895	0.28%
3–year data	0.915	0.23%

NOTE. — Kurtosis values of different WCM versions at scale R_9. The right column gives the probability of obtaining a higher or equal value in Gaussian simulations.

have 0.08% again at scale R_7. The deviation from Gaussianity is localised in the southern hemisphere because *the Spot* is responsible for it (see C05).

3.2. *Maximum statistic*

Given n individual observations X_i, Max is defined as the largest (absolute) observation :

$$Max_n = max\{|X_1|, |X_2|, \ldots, |X_n|\}.$$

The very cold minimum temperature of *the Spot*, was shown to deviate from the Gaussian behaviour in V04. In this work and in C05, C06 the minimum temperature estimator was used to characterise *the Spot* whereas in CJT the chosen estimator was Max. As Max is a classical and more conservative estimator, we will use it in the present paper instead of the minimum temperature. Our n observations correspond to values in real or wavelet space (normalized to zero mean and dispersion one). *The Spot* appears to be the maximum absolute observation of the data at scales between 200 and 400 arcmin. In Figure 4, the 1–year and 3–year WMAP data values of Max are compared to those obtained from the simulations. As for the kurtosis, both data releases show very similar results. The data lie outside the 1% acceptance interval at scales R_9 and R_{10}. The 3–year data show slightly higher values than the 1–year data at these scales. In particular, the upper tail probability for the 1–year data was 0.56%, whereas for the 3–year data we obtain 0.38% at scale R_9.

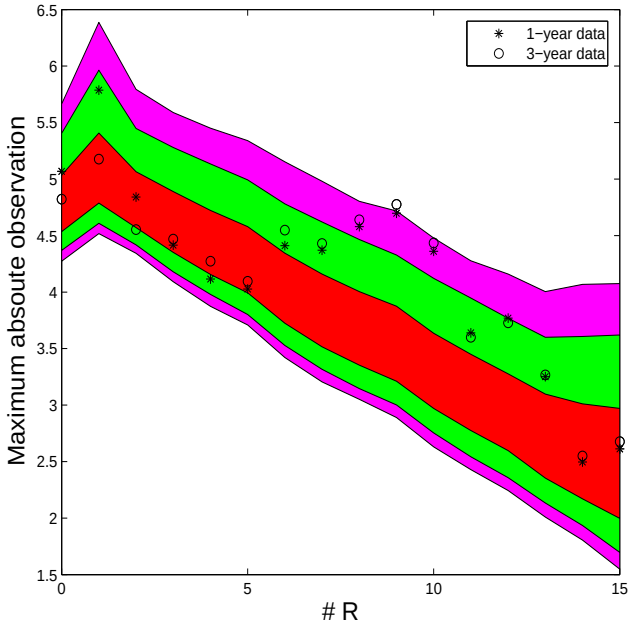

FIG. 4.— Maximum absolute observation versus the 15 wavelet scales. Again the circles represent the 3–year data and the asterisks the 1–year data. The bands represent the acceptance intervals as in previous figures.

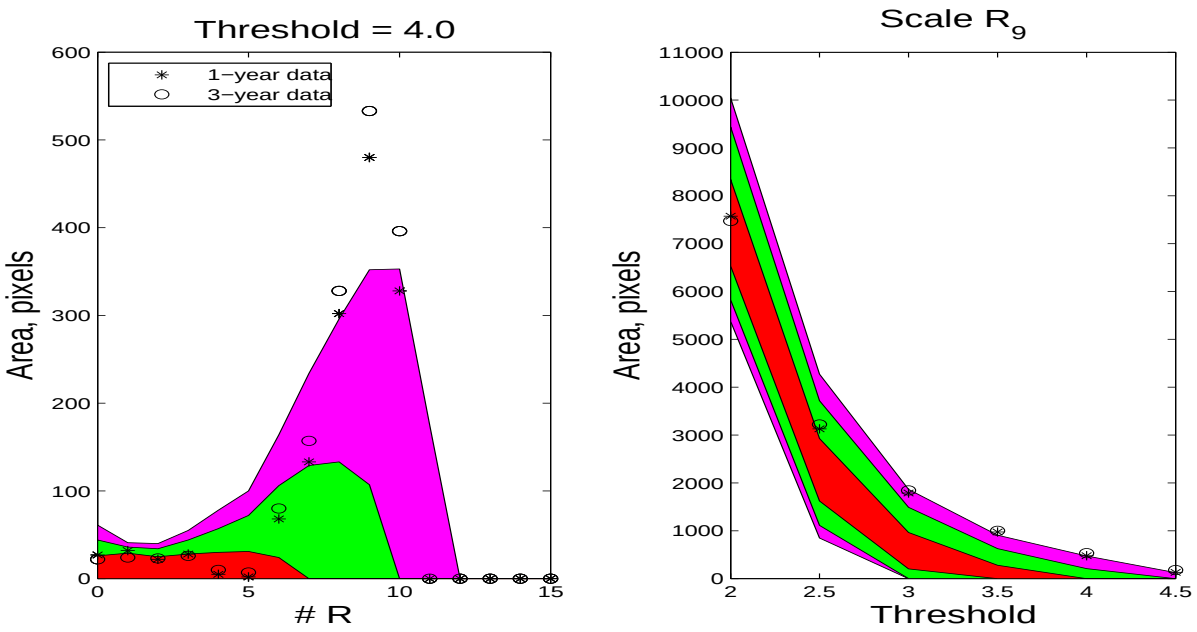

FIG. 5.— The left panel shows the cold Area in pixels, at threshold 4.0 versus the number of the scale. In the right panel the cold Area is represented versus the thresholds, while the scale is fixed at R_9. As in previous figures the asterisks represent the 1–year and the circles the 3–year data. The bands represent the acceptance intervals as in Figure 2

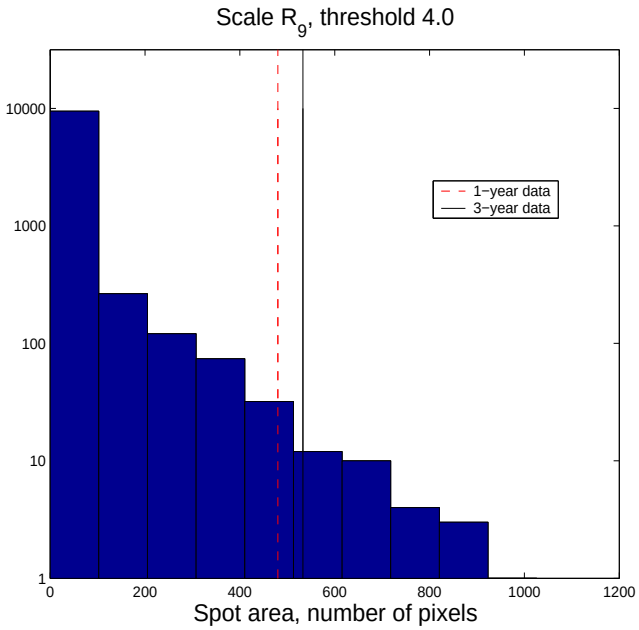

FIG. 6.— Histogram of all biggest spots of the simulations at threshold 4.0 and scale R_9. The dashed vertical line represents *the Spot* in the 1–year data and the solid one represents *the Spot* in the 3–year data.

TABLE 2
UPPER TAIL PROBABILITIES FOR THE AREA OF *the Spot* AT SCALE R_9

threshold	probability 1–year data	probability 3–year data
3.0	0.68%	0.63%
3.5	0.36%	0.37%
4.0	0.34%	0.27%
4.5	0.44%	0.35%

TABLE 3
UPPER TAIL PROBABILITIES FOR THE VOLUME OF *the Spot*, SCALE R_9

threshold	probability 1–year data	probability 3–year data
3.0	0.51%	0.45%
3.5	0.33%	0.38%
4.0	0.32%	0.27%
4.5	0.44%	0.35%

3.3. *Area*

We define the hot Area as the number of pixels above a given threshold ν and the cold Area as the number of pixels below a given threshold $-\nu$. The threshold is given in units of the dispersion of the considered map.

In C05 the total cold Area of the 1–year data was found to deviate from the Gaussian behaviour at scales R_8 and R_9 and thresholds above 3.0 (see Figures 1 and 2 in C05).

C05 found that the large cold Area of *the Spot* was responsible for this deviation. Such a big spot was very unlikely to be found under the Gaussian model at several thresholds (see Table 2 of C05).

In the present paper we will define the Area as the maximum between hot and cold Area at a given threshold and scale. As for the Max estimator, we obtain in this way a more conservative estimator since *the Spot* will be compared to the biggest spot in each simulation no

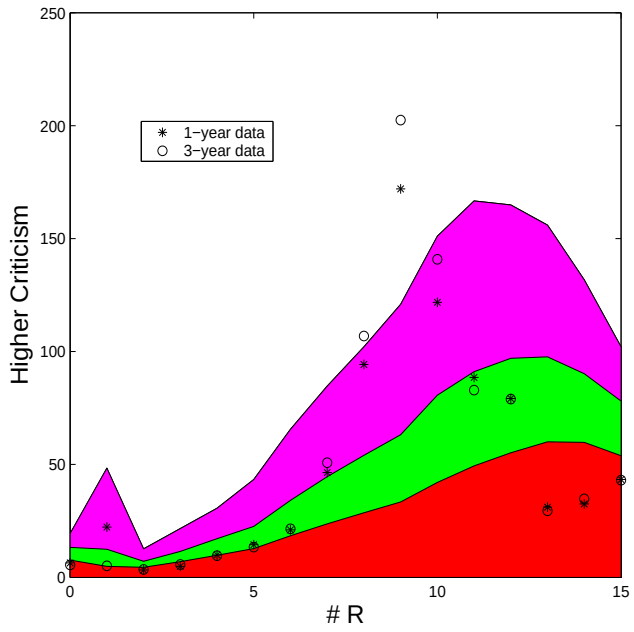

FIG. 7.— Higher Criticism values of the 1–year WCM (asterisks) and the 3–year WCM (circles). The acceptance intervals are plotted as in previous figures.

matter if it is a cold or a hot spot.

However the Area still deviates from the Gaussian behaviour as can be seen in Figure 5. The most significant deviation is again found at scale R_9 and thresholds above 3.0.

Figure 6 shows the histogram of the biggest spot of each simulation compared to the 1–year and 3–year Area of *the Spot* at scale R_9 and threshold 4.0. *The Spot* is more prominent in the 3–year data and only very few simulations show bigger spots. The upper tail probabilities obtained at scale R_9 for 1–year and 3–year data are presented in table 2. As in the previous estimators, the 3–year data are in general slightly more significant. The new and more conservative definition of the Area estimator reduces the upper tail probability of *the Spot* although it is still widely below 1%.

3.4. *Volume*

From the previous subsections we know that *the Spot* is extremely cold and it has a large Area at thresholds above 3.0. The best estimator to characterise *the Spot* would be therefore the volume. Hence we define the volume referred to a particular threshold as the sum of the temperatures of the pixels conforming a spot at this threshold. In Table 3 we compare the probability of finding a spot with higher or equal Volume as the data, assuming the Gaussian hypothesis. The values are very similar to those obtained for the Area estimator. Values for the Volume are slightly more significant and they show less variations with the threshold.

3.5. *Higher Criticism*

The HC statistic proposed by Donoho & Jin (2004) was designed to detect deviations from Gaussianity that are caused by either a few extreme observations or a small

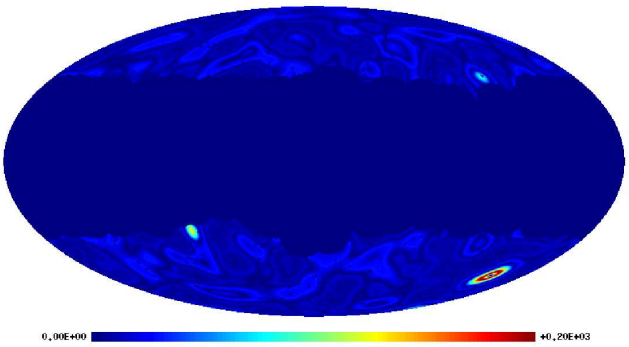

FIG. 8.— Higher Criticism of the 3–year WCM at scale R_9.

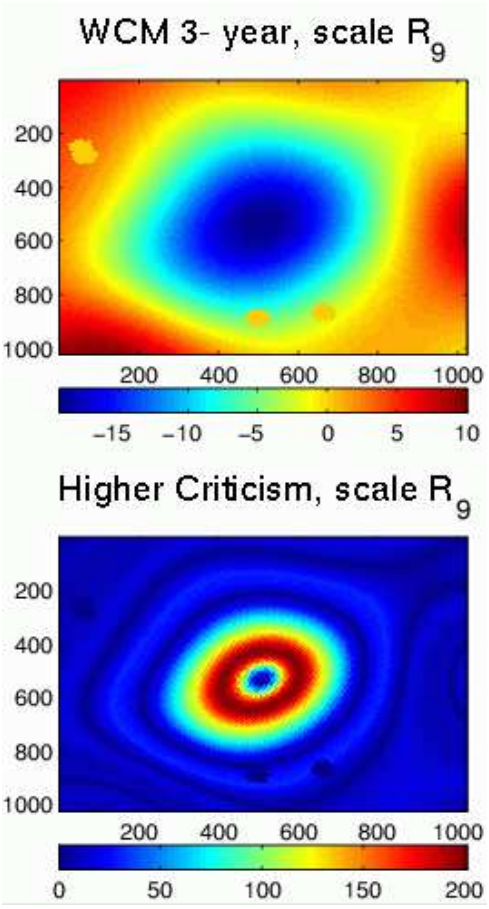

FIG. 9.— Image projected as in Figure 1, showing the 3–year WCM map (upper panel) and the Higher Criticism map (lower panel), both at scale R_9.

proportion of moderately extreme observations. Moreover, the statistic provides a direct method to locate these extreme observations by means of HC values calculated at every individual data point.

For a set of n individual observations X_i from a certain distribution (X_i normalized to zero mean and dispersion one), HC is defined as follows. The X_i observed values are first converted into p-values: $p_{(i)} = P\{|N(0,1)| > |X_i|\}$. After sorting the p-values in ascending order $p_{(1)} < p_{(2)} < \ldots < p_{(n)}$, we define the HC

at each pixel with p-value p_i, by:

$$HC_{n,i} = \sqrt{n}\left|\frac{i/n - p_{(i)}}{\sqrt{p_{(i)}(1-p_{(i)})}}\right|,$$

We compute the values of the HC statistic of the 3–year WCM in real and in wavelet space. The obtained values of the HC statistic are presented in Figure 7. These values correspond to the maximum of the HC values found at the individual pixels. As in previous figures, circles denote the results obtained from the 3–year WCM, asterisks those from the 1–year WCM and the bands represent the acceptance intervals. As one can see in the Figure, the data in wavelet space are not compatible with Gaussian predictions at scales R_8 and R_9 at the 99% c.l. This is in agreement with the result obtained by CJT for the 1–year WMAP data although there the HC values at scale R_8 were just below the 99% c.l. The upper tail probabilities for the 1–year and 3–year maximum HC values at scale R_9, are 0.56% and 0.36% respectively. The map of HC values at scale R_9 is presented in Figure 8. It is clear that the pixels responsible for the detected deviation from Gaussianity are located at the position of *the Spot*. Convolution with the wavelet causes the observed ring structure in the HC map. Figure 9 shows a blowout image of *the Spot* as it appears at scale R_9 in the wavelet map and in the HC map.

4. SIGNIFICANCE

In the previous section, the upper tail probabilities of each estimator at scale R_9 were given. All the considered estimators showed the lowest upper tail probability at scale R_9. However these are not rigorous measures of the significance of *the Spot*, since the number of performed tests is not taken into account. In this section we will recalculate the p-value of the deviation in the kurtosis found by V04 and discuss the issue of *a posteriori* significances.

When an anomaly is detected in a data set following a blind approach, usually several additional tests are performed afterwards to further characterize the anomaly. In most of these cases, the only reason these tests have been performed is the previous finding of the initial anomaly. If another anomaly would have been detected, other followup tests would have been performed. Hence these followup tests have not been performed blindly and should not be taken into account to calculate the significance of the initial detection.

This issue was already discussed in C06 and McEwen et al. (2005). Both papers recalculated the significance of the excess of kurtosis in the 1–year WCM found by V04. The excess of kurtosis was found performing a blind test, since no model was used and no previous findings conditioned the choice of the scales. Since 15 wavelet scales and two estimators (skewness and kurtosis) were considered, a total sum of 30 tests were performed. Three of these tests detected a strong deviation from Gaussianity. Scales R_7, R_8 and R_9 presented upper tail probabilities 0.67%, 0.40% and 0.38% in the 1–year data. This fact was taken into account in C06, but it was not by McEwen et al. (2005). The latter searched through the simulations in order to find how many of them showed a higher or equal deviation than the maximum deviation of the data, ignoring that the data showed a high deviation at two adjacent scales. The p-value found in this way was 4.97% whereas C06 obtained 1.91% taking into account that the data deviate at three consecutive scales. It is also interesting to note that, when both Galactic hemispheres were considered independently, C06 found a p-value of 0.69%, although this could be considered as a followup test.

TABLE 4
p-VALUES FOR DIFFERENT ESTIMATORS.

Estimators	p-value
kurtosis	0.86%
skewness + kurtosis	1.85%
Max	11.64%
Area 3.0	3.27%
Area 4.0	1.09%
Higher Criticism	3.48%

Some readers could find that the three-consecutive-scales criterion is an *a posteriori* choice since we look first at the data and given that they deviate at three consecutive scales, we then calculate from the simulations how probable this is. Therefore we should consider a new test which eliminates this *a posteriori* choice. We fix *a priori* a significance level which is the 1% acceptance interval given in all figures, and count for each estimator (skewness and kurtosis) how many scales lie outside, no matter if they are consecutive or not. Then we search through the simulations how many show at least that many scales outside the 1% acceptance interval as the data.

Applying this test to the 3–year WCM, we find that scales R_8 and R_9 lie outside the 1% acceptance interval and scale R_7 lies on the border for the kurtosis estimator as can be seen in Figure 2. Searching through the simulations how many deviate in three scales either in the skewness or in the kurtosis estimator, we find a p-value of 1.85%, which is still below the p-value obtained for the 1–year data with the three-consecutive-scales criterion.

As already discussed we should not include the followup tests in a rigorous significance analysis. However it is difficult to assess if some of these tests would have been performed or not without the first finding of V04. In fact, the area and maxima analyses are very intuitive and simple. If V04 had performed their blind analysis on those estimators instead of using skewness and kurtosis, then the significance would be different. We should distinguish between those tests which are clearly followup tests, because the only reason they have been performed is the initial detection, and other tests which just have been performed after the initial detection, but could have been performed before.

Hence we apply our new robustness test to kurtosis, Max, Area at thresholds 3.0 and 4.0 and Higher Criticism separately. Note that whereas the first two estimators are two-sided, the Area and Higher Criticism are one sided estimators. The p-values obtained in this way are listed in Table 4. The kurtosis and Area at threshold 4.0 show p-values around 1%, Higher Criticism and Area at threshold 3.0 around 3%. On the contrary the Max estimator does not show a significant deviation from Gaussianity according to this robustness test.

The most conservative and reliable value is the 1.85%

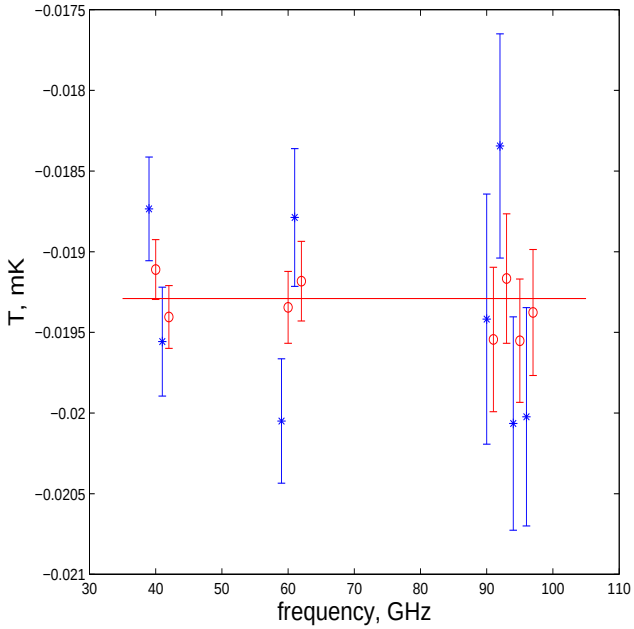

FIG. 10.— Frequency dependence of the temperature at the center of *the Spot* at scale R_9. Again the asterisks represent the 1–year data and the circles the 3–year data. The horizontal line shows the value of the 3–year WCM. The data at the same frequency have been slightly offset in abscissa for readability.

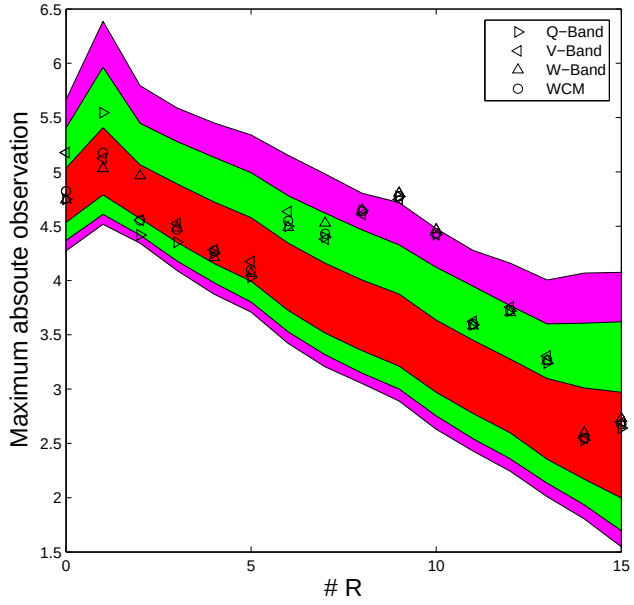

FIG. 11.— Maximum absolute observation for the Q, V and W bands, compared to the 3–year WCM values.

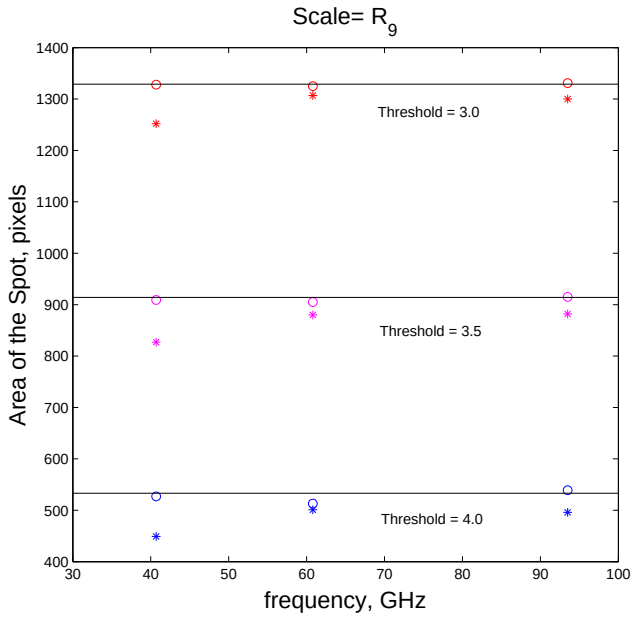

FIG. 12.— Frequency dependence of the Area of *the Spot* at scale R_9 and several thresholds. Asterisks represent the 1–year data and the circles the 3–year data. The 3–year WCM values are represented by horizontal lines.

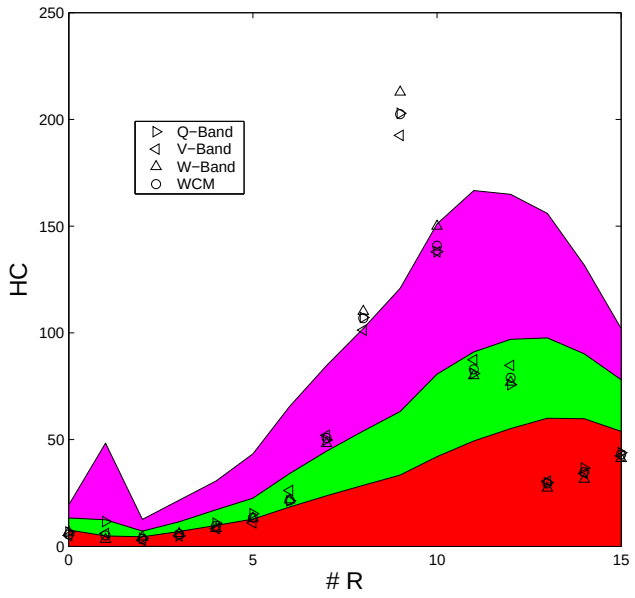

FIG. 13.— Higher Criticism values for the Q, V and W bands, compared to the 3–year WCM values.

figure since it is not suspicious of being obtained through *a posteriori* analyses. Nevertheless it is still noticeable that the followup tests performed in C05, C06, CJT and in the present paper, confirm the initial finding with a very similar significance. Even if strictly speaking these should not be taken into account for establishing the significance of *the Spot*, they confirm the robustness of the detection.

5. FREQUENCY DEPENDENCE

In this section we will analyse the frequency dependence of the previously analysed estimators. A flat frequency dependence is characteristic of CMB, whereas other emissions such as Galactic foregrounds show a strong frequency dependence. Figure 14 shows that the kurtosis has almost identical values at the three foreground cleaned channels, namely Q,V and W. Same behaviour was observed in the 1–year data (see Figure 7 in

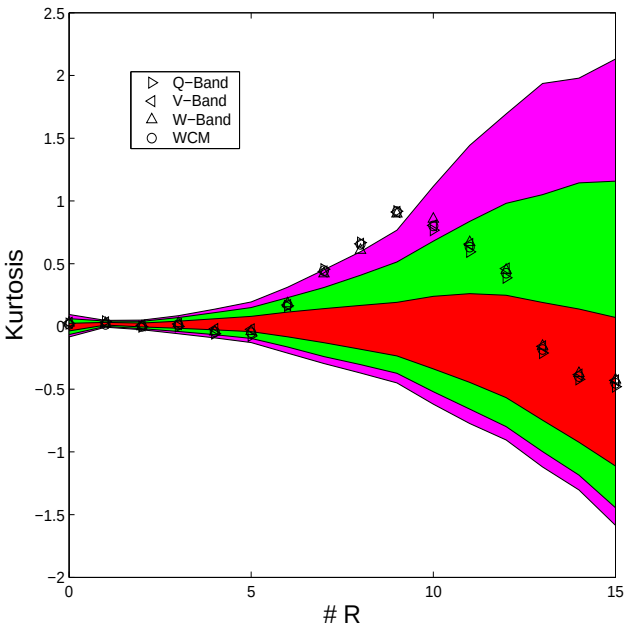

FIG. 14.— Kurtosis values for the Q, V and W bands, compared to the 3–year WCM values.

C06). Strong frequency dependent foreground emissions are unlikely to produce the detected excess of kurtosis.

The frequency dependence of the temperature at the center of *the Spot*, i.e. at the pixel where the temperature of *the Spot* is minimum in the WCM map, is presented in Figure 10. The error bars of the 1–year data have been estimated performing 1000 noise simulations as explained in section 5.1 of C06. As the noise variance is ≈ 3 times lower in the 3–year data, we estimate the new error bars simply by dividing the old ones by $\sqrt{3}$. No frequency dependence is found for the new data set in agreement with the results for the 1–year data. Max, Area and HC values at different frequencies (see Figure 11, Figure 12 and Figure 13) show a very low relative variation compared to the 3–year WCM.

All these results confirm the analysis performed in section 5 of C06 where the data were found to fit a flat CMB spectrum. The present analysis confirms the disagreement between the conclusions of C06 and those of the work of Liu & Zhang (2005) where Galactic foregrounds were considered to be the most likely source for non-Gaussian features found with spherical wavelets.

6. DISCUSSION

Spergel et al. (2006) enumerate several reasons to be cautious about the different anomalies found in the WMAP data: Galactic foregrounds or noise could be generating the non-Gaussianity, and in addition most of the claimed detections are based on *a posteriori* statistics. Also spatial variations of the noise variance and $1/f$ noise could affect some of the perfomed analyses. They suggest several tests to be done using difference maps (year 1 - year 2, year 2 - year 3, etc.) and multi-frequency data.

We have tried to address all those points for *the Spot*. The *a posteriori* analysis is one of the most important issues raised by Spergel et al. (2006), since it is very difficult to get completely rid of it. Most analyses perform many tests and it is not easy to assess how many of them are followup tests and which is the probability of finding an anomaly by chance. As discussed in section 4 a very careful analysis shows that *the Spot* remains statistically significant at least at the 98% confidence level, without using any *a posteriori* statistics.

In addition C06 proved that *the Spot* remained highly significant no matter which foreground reduction technique was used. These results are confirmed in the present paper. The new foreground reduction used in the 3–year data enhances slightly the significance of our detection. Moreover the multi-frequency analysis of the previous section shows an even flatter frequency dependence of *the Spot*.

As already discussed in previous sections the noise does not affect significantly our wavelet analysis. In fact the coadded 3–year results are very similar to those obtained with the 1–year data of the new data release. No significant cold spot is observed based on the analysis of the three difference maps (year 1 - year 2, year 2 - year 3, and year 1 - year 3). Moreover Figure 10 shows that even the particularly $1/f$ contaminated W4 Difference Assembly shows almost the same result as all the other Difference Assemblies.

7. CONCLUSIONS

In this paper we repeat the analyses that detected the non-Gaussian cold spot called *the Spot* at $(b = -57°, l = 209°)$ in wavelet space in the 1–year of WMAP data, using the recently released 3–year WMAP data. The previous works V04, C05, CJT and C06 found *the Spot* to deviate significantly from the Gaussian behaviour. *The Spot* was detected using several estimators, namely kurtosis, Area, Max and HC. This work confirms the detection applying all these estimators to the recently published 3–year WMAP data. At scale R_9, the upper tail probabilities of all these estimators when applied to the 3 year WMAP data are smaller than the corresponding ones for the first year WMAP data. This is mostly due to the improved foreground reduction of the data. We calculate the probability of finding such a deviation from Gaussianity considering only skewness and kurtosis since these were initially used by V04 following a blind approach. Therefore excluding followup tests which could be considered as *a posteriori* analyses we obtain a p-value of 1.85%. Moreover, *the Spot* appears to be almost frequency independent. This result reinforces the previous foreground analyses performed by C06. It is very unlikely that foregrounds are responsible for the non-Gaussian behaviour of *the Spot*. Comparing the WMAP single year sky maps, we conclude that the noise has a very low contribution to our wavelet analysis as already claimed in V04, C05. Future works will be aimed at finding the origin of *the Spot*. As discussed in the introduction several possibilities have been considered, based on Rees-Sciama effects (Rees & Sciama 1968, Martínez–González & Sanz 1990, Martínez–González et al. 1990) and inhomogenous or anisotropic universes. We are presently working on studying another: topological defects (Turok & Spergel 1990, Durrer et al. 1999) as textures could produce cold spots. New and more detailed analyses are required in order to answer that question.

The authors kindly thank R.B. Barreiro, L.M. Cruz-Orive and J.L. Sanz for very useful comments and R. Marco for computational support. MC thanks Spanish Ministerio de Educacion Cultura y Deporte (MECD) for a predoctoral FPU fellowship. PV thanks a I3P contract from the Spanish National Research Council (CSIC). MC, EMG and PV acknowledge financial support from the Spanish MCYT project ESP2004-07067-C03-01 and the use of the Legacy Archive for Microwave Background Data Analysis (LAMBDA). Support for LAMBDA is provided by the NASA Office of Space Science. This work has used the software package HEALPix (Hierarchical, Equal Area and iso-latitude pixelization of the sphere, http://www.eso.org/science/healpix), developed by K.M. Górski, E. F. Hivon, B. D. Wandelt, J. Banday, F. K. Hansen and M. Barthelmann; the visualisation program Univiewer, developed by S.M. Mingaliev, M. Ashdown and V. Stolyarov; and the CAMB and CMBFAST software, developed by A. Lewis and A. Challinor and by U. Seljak and M. Zaldarriaga respectively.

REFERENCES

Adler R. J., Bjorken J. D., Overduin J. M., 2006, gr-qc/0602102.
Bennett C.L., et al., 2003, ApJS, 148, 1.
Bennett C.L., et al., 2003, ApJS, 148, 97.
Bielewicz P., Eriksen H. K., Banday A. J., Górski K. M., Lilje P. B., 2005, ApJ, 635, 750B
Cabella P., Liguori M., Hansen F.K., Marinucci D.,Matarrese S., Moscardini L., Vittorio N., 2005, MNRAS, 358, 684.
Cayón L., Jin J., Treaster A., 2005, MNRAS, 362, 826.(CJT)
Cayón L., Banday A. J., Jaffe T., Eriksen H. K., Hansen F.K., Gorski K. M., Jin J., 2005, submitted to MNRAS, (astro-ph/0602023).
Chiang L. -Y., Naselsky P. D., Verkhodanov O. V., 2003, ApJ, 590, 65.
Chiang L-Y, Naselsky P.D., Coles P., 2006, (astro-ph/0603662).
Chyzy K.T., Novosyadlyj B., Ostrowski M., 2005, (astro-ph/0512020).
Coles P., Dineen P., Earl J., Wright D., 2004, MNRAS, 350, 989.
Copi C. J., Huterer D., Starkman G. D., 2004, Phys. Rev. D., 70, 043515.
Copi C. J., Huterer D., Schwarz D. J., Starkman G. D., 2005, submitted to MNRAS (astro-ph/0508047).
Cruz M., Martínez–González E., Vielva P., Cayón L., 2005, MNRAS, 356, 29. (C05).
Cruz M., Tucci M., Martínez–González E., Vielva P., 2006, accepted in MNRAS, (astro-ph/0601427). (C06).
Dineen P., Coles P., 2005, submitted to MNRAS (astro-ph/0511802).
Donoho D., Jin J., 2004, *Ann. Statist.*, 32, 962
Durrer R., 1999, New Astron. Rev., 43, 111.
Eriksen H. K., Banday A. J., Górski K. M., Lilje P. B., 2005, ApJ, 622, 58.
Eriksen H. K., Hansen F. K., Banday A. J., Górski K. M., Lilje P. B., 2004, ApJ, 605, 14.
Eriksen, H. K., Novikov, D. I., Lilje, P. B, Banday, A. J., Górski K. M., 2004, ApJ, 612, 64.
Górski K.M., Hivon E. F., Wandelt B. D., Banday J., Hansen F. K., Barthelmann M., 2005, ApJ 622, 759.
Hansen F.K., Cabella P., Marinucci D., Vittorio N., 2004, ApJL, 607, L67.
Hinshaw et al., 2006, submitted to ApJ, (astro-ph/0603451)
Inoue K. T., Silk J., 2006, (astro-ph/0602478)
Jaffe T. R., Banday A. J., Eriksen H. K., Górski K. M., Hansen F. K., 2005, ApJ, 629, 1.
Jaffe T. R., Hervik S., Banday A. J., Górski K. M., 2005, submitted to ApJ (astro-ph/0512433).
Komatsu E. et al. , 2003, ApJs, 148, 119.
Land K., Magueijo J., 2005a, MNRAS, 357, 994.
Land K., Magueijo J., 2005b, MNRAS, 362, 16.
Land K., Magueijo J., 2005d, MNRAS, 362, 838.
Larson D. L., Wandelt B. D., 2004, ApJ, 613, 85.
Larson D. L., Wandelt B. D., 2005, submitted to Phys. Rev. D. (astro-ph/0505046).
Liu X., Zhang S.N., 2005, ApJ, 633, 542.
Martínez–González E. & Sanz J. L., Silk, J., 1990, ApJL, 335, 5.
Martínez–González E. & Sanz J. L., 1990, MNRAS, 247, 473.
Martínez–González E., Gallegos J. E., Argüeso F., Cayón L. & Sanz J. L., 2002, MNRAS, 336, 22.
McEwen J. D., Hobson M. P., Lasenby A. N., Mortlock D. J., 2005, MNRAS, 359, 1583.
McEwen J. D., Hobson M. P., Lasenby A. N., Mortlock D. J., 2005, submitted to MNRAS (astro-ph/0510349).
Mukherjee P., Wang Y., 2004, ApJ, 613, 51.
de Oliveira-Costa A., Tegmark M., Zaldarriaga M., Hamilton A., 2004, Phys. Rev. D., 69, 63516.
Park C. G. 2004, MNRAS 349, 313-320.
Rees M. J. & Sciama D. W., 1968, Nature, 517, 611.
Schwarz D. J., Starkman G. D., Huterer D., and Copi C. J., 2004, Phys. Rev. Lett., 93, 221301.
Slosar A., Seljak U., 2004, Phys. Rev. D., 70, 8.
Spergel et al. 2006, submitted to ApJ, (astro-ph/0603449)
Tojeiro R., Castro P.G., Heavens A.F., Gupta S., 2005, submitted to MNRAS (astro-ph/0507096).
Tomita K., 2005, Phys. Rev. D, 72, 10.
Turok N. & Spergel D. N., 1990, Phys. Rev. Letters, 64, 2736
Vielva P., Martínez–González E., Barreiro R. B., Sanz J.L., Cayón L., 2004, ApJ, 609, 22. (V04).
Wiaux Y., Vielva P., Martínez–González E., Vandergheynst P., 2006, submitted to Phys. Rev. Letters.